

Valence-band photoemission and optical absorption in nickel compounds

Atsushi Fujimori* and Fujio Minami

National Institute for Research in Inorganic Materials, Sakura-mura, Niihari-gun, Ibaraki 305, Japan

(Received 21 February 1984)

Photoemission, optical-absorption, and isochromat spectra of NiO and NiCl₂ are studied theoretically by the consideration of configuration interactions within the metal-ligand cluster. It is shown that the satellites in the valence-band photoemission spectra contain significant d^7 final-state components produced by photoemission of a d electron from the largely d^8 -like ground state and that final states giving the main lines are predominantly d^8 -like resulting from ligand \rightarrow 3 d charge-transfer transitions following the d -electron emission. This identification differs markedly from the traditional one, according to which the main lines are due to d^7 final states and the satellites are produced by ligand \rightarrow 3 d shakeup transitions. The crystal-field splitting and the apparent reduction of Racah parameters are shown to be due to hybridization between different configurations. The resonance enhancement of the satellites rather than the main lines at the 3 p \rightarrow 3 d photoabsorption threshold is attributed partly to covalency and partly to the small number of 3 d holes in the nickel compounds as compared to other 3 d transition-metal compounds. Excitation energies for ligand p \rightarrow Ni 3 d charge-transfer optical absorption are calculated and it is shown that the fundamental absorption edge of NiO at ~ 4 eV is not due to the p \rightarrow d charge-transfer transitions. Instead, d \rightarrow d charge-transfer transitions are proposed as the origin of the NiO fundamental edge. Energy levels involved in the intra-atomic d \rightarrow d optical absorption are also calculated by the configuration-interaction approach and good agreement with experiment and energy levels calculated by the ligand-field theory is obtained. Finally the isochromat spectrum of NiO is discussed, based on the same approach.

I. INTRODUCTION

Electron correlation plays an important role in the electronic properties of narrow-band materials. In monoxides and dihalides of 3 d transition metals (Mn, Fe, Co, Ni, and Cu), electrons in the incomplete 3 d shell are thought to be localized due to strong electron-electron correlation. Paramagnetic energy-band calculations^{1,2} predict that they should be metallic, although they are actually insulators. Band calculations of NiO and MnO with antiferromagnetic spin structures have given insulating band gaps,³⁻⁶ but the gap energies are considerably smaller than the experimental values.^{3,5} Moreover, it has not been possible to give a band gap for FeO and CoO (Refs. 5 and 6). On the other hand, localized approaches such as the crystal-field or ligand-field (LF) theory⁷⁻⁹ have been successfully applied to the optical and magnetic properties. Optical absorption below the fundamental absorption edge is well described by the ligand-field theory, according to which optical transitions occur between crystal-field-split levels of the 3 d^n ion. The 3 d electrons are not completely localized, however: Electron transfer between the 3 d and ligand orbitals (covalency) and also between neighboring 3 d sites exists to some extent. The covalency effects have been studied theoretically by molecular-orbital calculations of metal-ligand complexes,¹⁰⁻¹² and have been demonstrated in the crystal-field splitting,¹⁰⁻¹² nuclear magnetic resonance,¹³⁻¹⁵ neutron diffraction,^{16,17} positron annihilation,¹⁸ etc.

Photoemission of valence electrons in strongly correlated systems usually exhibits many-body effects.^{19,20} In

fact, strong satellite emission has been observed for NiO (Refs. 21-25) and NiCl₂ (Refs. 23, 26, and 27) at 5-7 eV below the main lines. The main lines have been assigned to d^{n-1} final states produced by emission of a 3 d electron from the d^n ground state, and their multiplet structures have been interpreted in terms of the ligand-field theory, while the satellites have been attributed to 3 d^nL final states, where L denotes a ligand hole, resulting from ligand-to-3 d charge-transfer transitions accompanying the 3 d emission^{23,24} by analogy with the core-level spectra.^{23,28-30} However, recent resonant photoemission studies on NiO (Refs. 31 and 32) and transition-metal dichlorides³³ suggested that the above assignment of the valence-band spectra may not be entirely correct. These experiments showed that at the 3 p \rightarrow 3 d excitation threshold the satellite lines rather than the main lines are enhanced in the Ni and Co compounds while the main lines are enhanced in Mn and Fe chlorides. According to the theory of Davis,³⁴ d^{n-1} final states should be enhanced in resonant photoemission rather than the d^nL final states. Thus the previous identification of the valence-band spectra becomes questionable at least for Ni and Co compounds, and the valence-band photoemission of the 3 d transition-metal compounds must be reinterpreted by properly taking into account the charge-transfer effects. The valence-band x-ray photoemission spectroscopy (XPS) of Cu dihalides^{35,36} and the resonant photoemission of CuO (Ref. 37) have also suggested that the satellites are due to 3 d^{n-1} final states and that the main bands are due to ligand-to-3 d charge-transfer final states.

In order to study the valence-band photoemission in-

cluding the charge-transfer effects in the final states, we consider configuration interactions within the metal-ligand complex,³⁸ namely, interactions between states with different numbers of $3d$ electrons or ligand holes. Photoemission from Ce compounds (stable-valence Ce^{3+} and mixed-valence Ce) has previously been treated in a similar way.³⁹ In this paper, the valence-band photoemission, optical-absorption, and isochromat spectroscopies of NiO and NiCl_2 are studied with use of the configuration-interaction (CI) approach. The arrangement of this paper is as follows. In Sec. II a cluster model including electron correlation is described. In Secs. III and IV, calculated valence-band spectra and their resonance behaviors are presented. Optical absorption due to intra-atomic $d \rightarrow d$ transitions^{40,41} and charge-transfer transitions are studied using the same model in Secs. V and VI. The results of Sec. VI are used to discuss the origin of the fundamental absorption edge⁴²⁻⁴⁴ in NiO. In Sec. VII the isochromat or inverse photoemission spectrum⁴⁵ of NiO is interpreted. Finally in Sec. VIII we discuss implications of the present results on the valence-band satellites of Ni metal^{46,47} and metallic Ni compounds,³² where the satellites have been ascribed to two-hole bound states.⁴⁸⁻⁵¹ A summary of the results of Sec. III and calculations of spin-polarized spectra have been reported elsewhere.⁵²

II. CLUSTER MODEL WITH ELECTRON CORRELATION

Energy levels of the $3d^n$ ion in solids are different from those of the free ion in that the one-electron $3d$ level splits into crystal-field levels, and Coulomb and exchange interactions between $3d$ electrons, denoted by Slater F_2 and F_4 integrals or equivalently by Racah B and C parameters, are reduced from the free-ion values.^{7,8,53} These effects are explained by hybridization between the $3d$ and ligand orbitals, namely, by covalency.¹⁰⁻¹² In order to derive the covalency effects theoretically, molecular-orbital approaches of the metal-ligand complex have been applied, and reasonable crystal-field parameters and reduction of B and C have been obtained.¹⁰⁻¹² Another approach to the covalency effects has been the configuration-interaction study by Hubbard *et al.*,³⁸ who described the metal-ligand complex as mixed configurations of d^n and $d^{n-1}\underline{L}$ and derived the crystal-field splitting. The present model treats this type of configuration interactions in the photoemission final states as well as in the ground state.

A cluster NiO_6^{-10} (NiCl_6^{-4}), where a Ni atom is octahedrally (approximately octahedrally) coordinated by O (Cl) atoms, is considered. If we neglect the multiplicity of the d^n -ion energy levels and the ligand orbitals, the ground state is written as

$$\Psi_g = a_0 |d^8\rangle + a_1 |d^9\underline{L}\rangle, \quad (1)$$

where the first term represents the $\text{Ni}^{2+}(3d^8)$ ion and completely filled ligand orbitals, and the second term a charge-transfer state with $\text{Ni}^+(3d^9)$ and a ligand hole \underline{L} . Higher-order terms such as $d^{10}\underline{L}^2$ have been neglected, since these levels lie high enough to be neglected due to Coulomb repulsion between $3d$ electrons. We note that

the "ligand orbitals" mean exactly bonding orbitals between the Ni $4s, 4p$ and ligand orbitals rather than the pure ligand orbitals. In $3d$ transition-metal oxides, this type of mixing between the metal $4s, 4p$ orbitals and the O $2s$ and $2p$ orbitals has been found to be substantial.^{1,54} With use of the Ni $4s, 4p$ -ligand bonding orbitals we do not include explicitly the Ni $4s, 4p$ orbitals in the basis set, although in general charge transfer between the Ni $4s, 4p$ and ligand orbitals could occur during photoemission or in other spectroscopies. This type of charge transfer or interatomic polarization would screen changes in the $3d$ - or ligand-electron number and would result in relaxation of the energies of excited states. In the present model, this effect is implicitly taken into account by using adjustable parameters such as energy differences and overlap and transfer integrals between different configurations. In Eq. (1), $|a_1|^2$ is generally much smaller than $|a_0|^2$, since covalency is not large in the ground state.^{10-18,55,56} The Hamiltonian for the ground state is of the form

$$\tilde{H} = \begin{pmatrix} E_8 & v \\ v & E_8 + \delta E_A \end{pmatrix}, \quad (2)$$

where $E_8 = \langle d^8 | \tilde{H} | d^8 \rangle$ and $\delta E_A = E(d^8 \rightarrow d^9\underline{L}) = \langle d^9\underline{L} | \tilde{H} | d^9\underline{L} \rangle - \langle d^8 | \tilde{H} | d^8 \rangle$ is an energy required to move an electron from the ligand to $3d$ orbitals. $v = \langle d^8 | \tilde{H} | d^9\underline{L} \rangle$ is an effective transfer integral for the charge-transfer process. Thus the ground state is given by solving the secular equation

$$\det | \tilde{H} - E\tilde{S} | = 0, \quad (3)$$

where \tilde{S} is an overlap matrix.

Final states of the $3d$ photoemission are given by

$$\Psi_f = b_{f0} |d^7\rangle + b_{f1} |d^8\underline{L}\rangle + b_{f2} |d^9\underline{L}^2\rangle, \quad (4)$$

and the Hamiltonian is

$$\tilde{H} = \begin{pmatrix} E_7 & v' & 0 \\ v' & E_7 + \delta E_B & v'' \\ 0 & v'' & E_7 + \delta E_B + \delta E_C \end{pmatrix}, \quad (5)$$

where $\delta E_B = E(d^7 \rightarrow d^8\underline{L})$, $\delta E_C = E(d^8\underline{L} \rightarrow d^9\underline{L}^2)$, and v' and v'' are corresponding effective transfer integrals. E_7 is an energy required to remove an electron from the cluster and to place it at the Fermi level E_F (e.g., of the spectrometer). The $3d$ photoemission intensity for a final state Ψ_f is

$$I_f \propto |a_0 d_{f0} T_0 + a_1 b_{f1} T_1|^2, \quad (6)$$

where T_0 and T_1 are appropriate transition-matrix elements for the d -electron emission. Likewise, final states of isochromat spectroscopy are given by

$$\Psi_f = c_{f0} |d^9\rangle + c_{f1} |d^{10}\underline{L}\rangle. \quad (7)$$

So far we have neglected in Eqs. (1)–(7) multiplicity of the $3d$ and ligand orbitals. We then consider the crystal-field splitting of the Ni $3d$ orbitals into t_{2g} and e_g orbitals, and the multiplet splitting of the d^7 and d^8 ions due to intra-atomic Coulomb and exchange interactions. As for the ligand orbitals, molecular orbitals consisting of the $0\ 2s$ and $2p$ (Cl $3s$ and $3p$) orbitals are considered. In the

case of two-ligand-hole states $d^9\bar{L}^2$, correlation between the two holes should be included but, in this work, this is neglected for simplicity. Exchange interactions between 3d electrons and ligand holes are also neglected. Both in the ground state (1) and the final states (4) or (7), only hybridization between different configurations with the same total symmetry is allowed. For example, the ground state of the Ni²⁺ ion in a cubic crystal field is known to have a configuration $t_{2g}^6 e_g^2$ with the total symmetry of ${}^3A_{2g}$, and therefore only $d^9\bar{L}$ states with ${}^3A_{2g}$ symmetry appear in the second term of Eq. (1). The photoemission final states (4) have either ${}^4T_{1g}$, ${}^2T_{1g}$, or 2E_g symmetry after d -electron emission from the ${}^3A_{2g}$ ground state. Each final-state symmetry involves eigenstates and a Hamiltonian of the form (4) and (5). Ligand holes \bar{L} appearing in these formulas have either e_g or t_{2g} symmetry, the former originating from O 2s and 2p orbitals and the latter from only O 2p orbitals. The \bar{L} and \bar{L}^2 terms in Eqs. (1), (4), and (7) are thus replaced by summations over these ligand holes, so that the sizes of the matrices (2) and (5) increase correspondingly. We also consider configuration interactions within the d^7 states and those within the d^8 states: For d^7 , not only $t_{2g}^5 e_g^2$ and $t_{2g}^6 e_g$ configurations, which are reached by one-electron transitions from the ground state, but also $t_{2g}^4 e_g^3$ and $t_{2g}^3 e_g^4$ configurations are included, and, for d^8 , in addition to $t_{2g}^6 e_g^2$ and $t_{2g}^5 e_g^3$, $t_{2g}^4 e_g^4$ is considered.

Nondiagonal matrix elements of \tilde{H} and \tilde{S} , effective transfer and overlap integrals, were evaluated from linear-combination-of-atomic-orbitals (LCAO) parameters of NiO calculated by Mattheiss.¹ Diagonal matrix elements of \tilde{H} (δE_A , δE_B , and δE_C) are difficult to evaluate, since they involve total energies of virtual excited states for which various relaxation effects exist such as interatomic and intra-atomic polarization of Ni and ligand ions, screening of Coulomb interactions, etc.^{57,58} Therefore, we regarded these energies as adjustable parameters which are to be determined in a manner to reproduce the experimental spectra. Furthermore, the transfer and overlap integrals were multiplied by a common scale factor in order to give best fit to the experimental spectra. On the other hand, the experimental values of the B and C parameters for the free Ni²⁺ and Ni³⁺ ions⁵³ were used without modification. The crystal-field parameter Δ_{CF} and the reduction of B and C were obtained as a consequence of the covalency effects or the configuration interactions, as will be shown in the following sections.

III. SATELLITE STRUCTURES IN THE VALENCE-BAND PHOTOEMISSION SPECTRA

The electronic ground state of the NiO₆⁻¹⁰ cluster has the symmetry ${}^3A_{2g}$ (hereafter, the suffix g representing even parity is implicitly assumed when omitted) and is given by Eq. (1) or more explicitly by

$$\Psi_g({}^3A_2) = a_0 |t_{2g}^6 e_g^2 {}^3A_2\rangle + a_1 |t_{2g}^5 e_g^3 {}^3A_2\rangle + a_2 |t_{2g}^4 e_g^4 {}^3A_2\rangle, \quad (8)$$

where the first term is a d^8 state and the second and last terms are $d^9\bar{L}$ states with $\bar{L} = p_\sigma$ and $\bar{L} = \underline{s}_\sigma$, respectively.

p_σ and s_σ denote e_g -like molecular orbitals derived from O 2p and O 2s orbitals. $d^9\bar{p}_\pi$, where p_π stands for a t_{2g} -like 2p molecular orbital, is not allowed in the ${}^3A_{2g}$ -like ground state, since the t_{2g} levels are already filled in the first term of (8). The second and last terms of Eq. (8) are obtained by applying symmetry operations to $d^9\bar{L}$ states. The Hamiltonian (2) for the ${}^3A_{2g}$ symmetry is explicitly written as

$$\tilde{H} = \begin{pmatrix} E_8 + \Delta({}^3A_2) & \sqrt{2}v_\sigma & \sqrt{2}v_s \\ \sqrt{2}v_\sigma & E_8 + \delta E_A & 0 \\ \sqrt{2}v_s & 0 & E_8 + \delta E_A + \epsilon_p - \epsilon_s \end{pmatrix}, \quad (9)$$

where $\Delta({}^3A_2)$ is the energy of the ${}^3A_{2g}$ term of the d^8 configuration relative to the center of gravity of the d^8 multiplets and is given in terms of B and C . The $d^9\bar{L}$ states have no multiplet splitting. $\epsilon_p - \epsilon_s$ is the one-electron energy difference between ligand p (p_σ) and s orbitals. δE_A is exactly defined as $\delta E_A = E(d^8 \rightarrow d^9\bar{p}) \equiv E(t_{2g}^6 e^2 \rightarrow t_{2g}^5 e^3 p_\sigma)$ by setting $B, C \rightarrow 0$. The value of \tilde{E}_8 in (9) was determined in such a way to make the ground-state energy 0. v_σ and v_s (and v_π , which appears in Table I) are effective transfer integrals and are given by

$$v_\sigma = -\sqrt{3}(pd\sigma)', \quad (10a)$$

$$v_s = \sqrt{3}(sd\sigma)', \quad (10b)$$

$$v_\pi = -2(pd\pi)', \quad (10c)$$

where $(pd\sigma)'$, $(sd\sigma)'$, and $(pd\pi)'$, are related to LCAO parameters $(pd\sigma)$, $(sp\sigma)$, $(pd\pi)$, S_σ , S_s , and S_π in Ref. 1 as

$$(pd\sigma)' = (pd\sigma) + S_\sigma X, \quad (11a)$$

$$(sd\sigma)' = (sd\sigma) + S_s X, \quad (11b)$$

$$(pd\pi)' = (pd\pi) + S_\pi X. \quad (11c)$$

Here X is an energy-scale shift⁵⁹ which makes the O 2p (Cl 3p) band at several eV below E_F as observed in the spectra.

Effective overlap integrals s_σ , s_s , and s_π in

$$\tilde{S} = \begin{pmatrix} 1 & \sqrt{2}s_\sigma & \sqrt{2}s_s \\ \sqrt{2}s_\sigma & 1 & 0 \\ \sqrt{2}s_s & 0 & 1 \end{pmatrix}, \quad (12)$$

are given in terms of overlap integrals S_σ , S_s , and S_π in Ref. 1 in a way similar to Eq. (10).

As final states of d -electron photoemission, ${}^4T_{2g}$, ${}^2T_{2g}$, and 2E_g are allowed. An explicit form of the Hamiltonian for each of them includes $d^8\bar{L}$ and $d^9\bar{L}\bar{L}'$ configurations with $L, L' = p_\sigma, p_\pi, s$, and also various d^7 and d^8 configurations. The basis functions and the Hamiltonians for these final states are presented in Table I.

Transition-matrix elements for photoemission from the d^8 ion, namely, matrix elements between d^8 and d^7 states, have been derived by the fractional parentage method.^{27,60,61} In this work, we need also matrix elements between $d^9\bar{L}$ and $d^8\bar{L}$. These are listed in Table II. With use of formulas of the type of Eq. (6), photoemission in-

TABLE I. Basis functions and Hamiltonians for the NiO_6^{-9} (NiCl_6^{-3}) cluster, which give final states of 3d-electron photoemission. The symmetry of p_σ , p_π , and s is 2E_g , ${}^2T_{2g}$, and 2E_g , respectively. The overlap matrices are given by setting $v_\sigma \rightarrow s_\sigma$, $v_\pi \rightarrow s_\pi$, and $v_s \rightarrow s_s$ in the Hamiltonians and other nondiagonal and diagonal elements to be 0 and 1, respectively. $P = E_7 + (32 + \frac{2}{3})B - (16 + \frac{1}{3})C$; $\Delta = \epsilon_e - \epsilon_t$; $Q = E_7 + \delta E_A + (43 + \frac{5}{9})B - (21 + \frac{7}{9})C$; $Q' = Q + \epsilon_p - \epsilon_s$; $R = E_7 + \delta E_A + \delta E_B$; $R' = R + \epsilon_p - \epsilon_s$; $R'' = R + 2(\epsilon_p - \epsilon_s)$; $\delta = \sqrt{2}[(pp\pi) - (pp\sigma)]$.

(a) 2E_g symmetry

$$\begin{aligned}
\varphi_1 &= |t_2^6 e^2 E\rangle, \quad \varphi_2 = |t_2^4 ({}^1E) e^3 {}^2E\rangle, \quad \varphi_3 = |t_2^4 ({}^1A_1) e^3 {}^2E\rangle \\
\varphi_4 &= |t_2^3 e^4 {}^2E\rangle, \quad \varphi_5 = |t_2^6 e^2 ({}^1A_1) p_\sigma {}^2E\rangle, \quad \varphi_6 = |t_2^6 e^2 ({}^3A_1) p_\sigma {}^2E\rangle \\
\varphi_7 &= |t_2^6 e^1 p_\sigma {}^2E\rangle, \quad \varphi_8 = |t_2^4 ({}^1A) e^4 p_\sigma {}^2E\rangle, \quad \varphi_9 = |t_2^4 ({}^1E) e^4 p_\sigma {}^2E\rangle \\
\varphi_{10} &= |t_2^6 e^2 ({}^1A_1) s^2 E\rangle, \quad \varphi_{11} = |t_2^6 e^2 ({}^3A_2) s^2 E\rangle, \quad \varphi_{12} = |t_2^6 e^2 ({}^1E) s^2 E\rangle \\
\varphi_{13} &= |t_2^4 ({}^1A) e^4 s^2 E\rangle, \quad \varphi_{14} = |t_2^4 ({}^1E) e^4 s^2 E\rangle, \quad \varphi_{15} = |t_2^6 e^3 p_\sigma^2 ({}^1A_1) {}^2E\rangle \\
\varphi_{16} &= |t_2^6 e^3 [s p_\sigma] ({}^1A_1) {}^2E\rangle, \quad \varphi_{17} = |t_2^6 e^3 s^2 ({}^1A_1) {}^2E\rangle \\
H_{1,1} &= P - 36B + 18C, \quad H_{2,2} = P - 29B + 17C + 2\Delta \\
H_{3,3} &= P - 20B + 20C + 2\Delta, \quad H_{4,4} = P - 34B + 17C + 3\Delta \\
H_{5,5} &= Q - 34B + 25C, \quad H_{6,6} = Q - 50B + 21C \\
H_{7,7} &= Q - 42B + 23C, \quad H_{8,8} = Q - 32B + 26C + 2\Delta \\
H_{9,9} &= Q - 41B + 23C + 2\Delta, \quad H_{10,10} = Q' - 34B + 25C \\
H_{11,11} &= Q' - 50B + 21C, \quad H_{12,12} = Q' - 42B + 23C \\
H_{13,13} &= Q' - 32B + 26C + 2\Delta, \quad H_{14,14} = Q' - 41B + 23C + 2\Delta \\
H_{15,15} &= R, H_{16,16} = R', \quad H_{17,17} = R'' \\
H_{1,2} &= 2\sqrt{3}B, \quad H_{1,3} = \sqrt{3}(2B + C), \quad H_{2,3} = 10B \\
H_{2,4} &= -3\sqrt{2}B, \quad H_{3,4} = -6\sqrt{2}B, \quad H_{1,5} = (1/\sqrt{2})v_\sigma \\
H_{1,6} &= \sqrt{3/2}v_\sigma, \quad H_{1,7} = -v_\sigma, \quad H_{5,8} = \sqrt{6}(2B + C) \\
H_{7,9} &= -2\sqrt{3}B, \quad H_{1,10} = (1/\sqrt{2})v_s, \quad H_{1,11} = \sqrt{3/2}v_s \\
H_{1,12} &= -v_s, \quad H_{10,13} = \sqrt{6}(2B + C), \quad H_{12,14} = -2\sqrt{3}B \\
H_{5,15} &= -(1/2)v_\sigma, \quad H_{6,15} = (\sqrt{3}/2)v_\sigma, \quad H_{7,15} = -(1/\sqrt{2})v_\sigma \\
H_{5,16} &= -(1/2\sqrt{2})v_s, \quad H_{6,16} = \frac{1}{2}\sqrt{3/2}v_s, \quad H_{7,16} = -\frac{1}{2}v_s \\
H_{10,16} &= -(1/2\sqrt{2})v_\sigma, \quad H_{11,16} = \frac{1}{2}\sqrt{3/2}v_\sigma, \quad H_{12,16} = -\frac{1}{2}v_\sigma \\
H_{15,16} &= 2\sqrt{2}v_s, \quad H_{10,17} = -\frac{1}{2}v_s, \quad H_{11,17} = (\sqrt{3}/2)v_s \\
H_{12,17} &= -(1/\sqrt{2})v_s
\end{aligned}$$

(b) ${}^2T_{1g}$ symmetry

$$\begin{aligned}
\varphi_1 &= |t_2^5 e^2 ({}^3A_2) {}^2T_1\rangle, \quad \varphi_2 = |t_2^5 e^2 ({}^1E) {}^2T_1\rangle, \quad \varphi_3 = |t_2^4 ({}^1T_2) e^3 {}^2T_1\rangle \\
\varphi_4 &= |t_2^4 ({}^3T_1) e^3 {}^2T_1\rangle, \quad \varphi_5 = |t_2^3 e^4 {}^2T_1\rangle, \quad \varphi_6 = |t_2^5 [e^3 p_\sigma] ({}^3A_2) {}^2T_1\rangle \\
\varphi_7 &= |t_2^6 e^2 ({}^3A_2) p_\pi {}^2T_1\rangle, \quad \varphi_8 = |t_2^5 [e^3 s] ({}^3A_2) {}^2T_1\rangle \\
\varphi_9 &= |t_2^5 e^4 p_\sigma^2 ({}^3A_2) {}^2T_1\rangle, \quad \varphi_{10} = |t_2^6 [e^3 p_\sigma] ({}^3A_2) p_\pi {}^2T_1\rangle \\
\varphi_{11} &= |t_2^5 e^4 [s p_\sigma] ({}^3A_2) {}^2T_1\rangle, \quad \varphi_{12} = |t_2^6 [e^3 s] ({}^3A_2) p_\pi {}^2T_1\rangle \\
\varphi_{13} &= |t_2^5 e^4 s^2 ({}^3A_2) {}^2T_1\rangle \\
H_{1,1} &= P - 34B + 17C + \Delta, \quad H_{2,2} = P - 30B + 17C + \Delta \\
H_{3,3} &= P - 34B + 17C + 2\Delta, \quad H_{4,4} = P - 28B + 17C + 2\Delta \\
H_{5,5} &= P - 34B + 17C + 3\Delta, \quad H_{6,6} = Q - 41B + (22 + \frac{1}{2})C + \Delta \\
H_{7,7} &= Q - 50B + 21C - \delta, \quad H_{8,8} = Q' - 41B + (22 + \frac{1}{2})C + \Delta \\
H_{9,9} &= R + \Delta, \quad H_{10,10} = R - \delta, \quad H_{11,11} = R' + \Delta \\
H_{12,12} &= R' - \delta, \quad H_{13,13} = R'' + \Delta, \quad H_{1,2} = 2\sqrt{3}B \\
H_{1,3} &= -3B, \quad H_{1,4} = 3B, \quad H_{2,3} = -\sqrt{3}B \\
H_{2,4} &= 3\sqrt{3}B, \quad H_{2,5} = -2\sqrt{3}B, \quad H_{3,4} = -3B \\
H_{3,5} &= 3B, \quad H_{4,5} = -3B, \quad H_{1,6} = \sqrt{2}v_\sigma \\
H_{1,7} &= v_\pi, \quad H_{1,8} = \sqrt{2}v_s, \quad H_{6,9} = \sqrt{2}v_\sigma \\
H_{6,10} &= v_\pi, \quad H_{6,11} = v_s, \quad H_{7,10} = \sqrt{2}v_\sigma \\
H_{7,12} &= \sqrt{2}v_s, \quad H_{8,11} = v_\sigma, \quad H_{8,12} = v_\pi \\
H_{8,13} &= \sqrt{2}v_s
\end{aligned}$$

TABLE I. (Continued).

(c) ${}^4T_{1g}$ symmetry	
$\varphi_1 = t_2^5 e^2 ({}^3A_2) {}^4T_1\rangle$	$\varphi_2 = t_2^4 ({}^3T_1) e^3 {}^4T_1\rangle$
$\varphi_3 = t_2^5 [e^3 p_\sigma] ({}^3A_2) {}^4T_1\rangle$	$\varphi_4 = t_2^6 e^2 ({}^3A_2) p_\pi {}^4T_1\rangle$
$\varphi_5 = t_2^5 [e^3 \underline{x}] ({}^3A_2) {}^4T_1\rangle$	$\varphi_6 = t_2^5 e^4 p_\sigma^2 ({}^3A_2) {}^4T_1\rangle$
$\varphi_7 = t_2^6 [e^3 p_\sigma] ({}^3A_2) p_\pi {}^4T_1\rangle$	$\varphi_8 = t_2^5 e^4 [s p_\sigma] ({}^3A_2) {}^4T_1\rangle$
$\varphi_9 = t_2^6 [e^3 \underline{x}] ({}^3A_2) p_\pi {}^4T_1\rangle$	$\varphi_{10} = t_2^5 e^4 \underline{x}^2 ({}^3A_2) {}^4T_1\rangle$
$H_{1,1} = P - 40B + 14C + \Delta$	$H_{2,2} = P - 31B + 14C + 2\Delta$
$H_{3,3} = Q - 44B + 21C + \Delta$	$H_{4,4} = Q - 50B + 21C - \delta$
$H_{5,5} = Q' - 44B + 21C + \Delta$	$H_{6,6} = R + \Delta$
$H_{7,7} = R - \delta$	$H_{8,8} = R' + \Delta$
$H_{9,9} = R' - \delta$	
$H_{10,10} = R'' + \Delta$	$H_{1,2} = 6B$
$H_{1,3} = \sqrt{2}v_\sigma$	
$H_{1,4} = v_\pi$	$H_{1,5} = \sqrt{2}v_s$
$H_{3,6} = \sqrt{2}v_\sigma$	
$H_{3,7} = v_\pi$	$H_{3,8} = v_s$
$H_{4,7} = \sqrt{2}v_\sigma$	
$H_{4,9} = \sqrt{2}v_s$	$H_{5,8} = v_\sigma$
$H_{5,9} = v_\pi$	
$H_{5,10} = \sqrt{2}v_s$	

tensities were calculated. It is noted that the cross-section difference between t_{2g} and e_g emission as introduced in ligand-field calculations⁶² is not required here, because our d orbitals are purely Ni $3d$ -like whereas in the ligand-field theory the t_{2g} and e_g orbitals are admixture of the $3d$ and ligand orbitals with different degrees of hybridization.

δE_A in Eq. (2) or (9) and δE_B and δE_C in Eq. (5) are thus left as free parameters which are to be determined in such a way to give best fit to the experimental spectra. For NiO, the transfer and overlap integrals were also multiplied by a factor $f=1.13$ in order to obtain best results. Spectra were calculated for various sets of δE_A , δE_B , and δE_C by varying them by an interval of 0.5 eV around the roughly estimated values (see below). Thus, excellent agreement with the XPS spectrum of NiO (Ref. 63) was obtained as in Fig. 1. In the figure, a spectrum calculated using the ligand-field theory is also shown, for which B and C are smaller than the Ni³⁺ free-ion values by more than 30% and the crystal-field parameter $\Delta_{CF} \sim 1$ eV has been introduced. There one can see that the satellite as well as the main lines are well reproduced by the spectrum calculated by the configuration-interaction scheme. The

parameters thus determined are listed in Table III together with other parameters used in the calculation. The calculated spectrum has been convoluted by a Lorentzian function whose width increases with increasing binding

TABLE II. Reduced transition-matrix elements for $3d$ photoemission from the NiO₆⁻¹⁰ (NiCl₆⁻⁴) cluster. Matrix elements between s -hole states are the same as those for the p -hole states listed here.

$$\begin{aligned}
 \langle t_2^5 e^2 {}^3A_2 || e || t_2^6 e^2 E \rangle &= \sqrt{6} \\
 \langle t_2^5 e^3 p_\sigma {}^3A_2 || e || t_2^6 e^2 ({}^1A_1) p_\sigma^2 E \rangle &= \sqrt{3/2} \\
 \langle t_2^5 e^3 p_\sigma {}^3A_2 || e || t_2^6 e^2 ({}^3A_1) p_\sigma^2 E \rangle &= 1\sqrt{2} \\
 \langle t_2^5 e^3 p_\sigma {}^3A_2 || e || t_2^6 e^2 ({}^1E) p_\sigma^2 E \rangle &= -\sqrt{3} \\
 \langle t_2^5 e^2 {}^3A_2 || t_2 || t_2^3 e^2 ({}^3A_2) {}^2T_1 \rangle &= -\sqrt{6} \\
 \langle t_2^5 e^3 p_\sigma {}^3A_2 || t_2 || t_2^3 [e^3 p_\sigma] ({}^3A_1) {}^2T_1 \rangle &= -\sqrt{6} \\
 \langle t_2^5 e^2 {}^3A_2 || t_2 || t_2^3 e^2 {}^4T_1 \rangle &= 2\sqrt{3} \\
 \langle t_2^5 e^3 p_\sigma {}^3A_2 || t_2 || t_2^3 [e^3 p_\sigma] ({}^3A_1) {}^4T_1 \rangle &= 2\sqrt{3}
 \end{aligned}$$

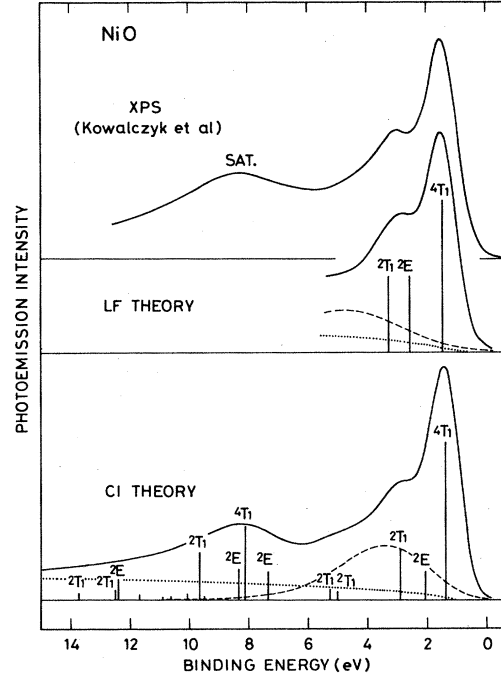


FIG. 1. Valence-band photoemission spectrum of NiO calculated by the configuration-interaction (CI) theory. The top panel shows the experimental XPS spectrum from Ref. 63. Binding energies have been shifted so as to be consistent with the reference level of Ref. 31. Multiplet of the d^7 final state calculated by the ligand-field (LF) theory ($B=0.09$ eV, $C=0.42$ eV, $\Delta_{CF}=0.93$ eV without configuration interactions within the d^7 configurations) are also indicated. The dashed line shows emission from the O $2p$ band, and the dotted line illustrates a background. For parameters used in the calculation, see Table III and text.

TABLE III. Parameters used in the calculation of the valence-band photoemission spectra of NiO (Fig. 1) and NiCl₂ (Fig. 3). Energies are in electron volts.

	NiO	NiCl ₂
Racah parameters ^a		
Ni ⁺² B	0.127	
C	0.601	
Ni ⁺³ B	0.138	
C	0.676	
Transfer and overlap integrals ^b		
(pdσ)	-1.036	
(pdπ)	0.475	
(sdσ)	-1.206	
S _σ	0.0531	
S _π	-0.0305	
S _s	0.0427	
(pps)	0.381	
(ppπ)	-0.063	
Atomic orbital energies ^c		
ε _e	5.09	
ε _e - ε _{t₂}	-0.5	
ε _p	-1.01	
ε _p - ε _s	16	11
Adjusted parameters ^d		
δE _A	4.0	2.5
δE _B	-3.5	-4.0
δE _C	1.0	0.5
E ₇	9.0	9.5
f	1.13	0.95
E _p	4.0	4.3
W _p	2.5	2.8
I _p	0.4	1.8
G	0.9	1.3
α	0.34	0.28

^aReference 53.

^bReference 1.

^cReference 1, except for ε_p - ε_s, which was taken from Refs. 21-23, and ε_e - ε_{t₂}, which was taken to be close to the diagonal value of Ref. 10 (-0.33 eV). In calculating the spectra, ε_e, ε_{t₂}, ε_p, and ε_s were shifted from these values with ε_e - ε_{t₂} and ε_p - ε_s fixed, as is described in the text.

^dE_p: binding energy of the center of the O 2p (Cl 3p) band relative to E_F; W_p, full width at half maximum (FWHM) of the Gaussian representing the O 2p (Cl 3p) band without instrumental and lifetime broadening. The Gaussian has been truncated for binding energies E_B lower than E₀, where E₀ is the lower binding-energy limit of the 3d lines; I_p, O 2p (Cl 3p)-to-Ni 3d relative intensity; G, FWHM of the Gaussian resolution function representing instrumental resolution; α (Lorentzian FWHM) = α(E_B - E₀).

energy in order to account for lifetime broadening and by a Gaussian resolution function representing instrumental resolution. A smoothly rising background proportional to the integrated intensity has been assumed. Emission from the O 2p band approximated by a broad Gaussian line shape centered at a binding energy of about 4 eV has been superimposed.

Figure 2 shows the configuration components of the spectral lines. The ligand-field theory (Fig. 1) is based on the assignment that the main lines at 1-4 eV are due to d⁷ final states and that the satellite at ~8 eV is due to d⁸L final states produced by the ligand-to-3d shakeup process. One can see from Fig. 2, however, that the main lines are predominantly d⁸L-like and the satellites lines have nearly equal d⁸L and d⁷ characters. There is also considerable mixing of the d⁹L² configuration into the main and satellite lines.

The value δE_A ≈ 4 eV thus determined seems consistent with those of Cu dihalides by analyses of the core-level satellites,³⁵ considering the electronegativities of the constituent elements: δE_A ~ 4 eV for CuF₂, δE_A ~ 2 eV for CuCl₂, etc., have been obtained. With use of this δE_A for NiO, the ground state is calculated to be a mixture of 92% d⁸ and 26% d⁹L configurations with an overlap population -18%. The negative overlap population corresponds to the fact that in the one-electron molecular-orbital picture the "3d" levels are antibonding combinations of the 3d and ligand orbitals.¹⁰ If the overlap part is divided equally into the d⁸ and d⁹L parts, the number of the 3d electrons in NiO is calculated to be 8.22 in agreement with that estimated from the neutron diffraction (8.2).¹⁷

δE_A may be represented as δE_A ≈ ε_d - ε_p + U - u, where -ε_d and -ε_p are ionization energies of the Ni 3d and O 2p orbitals from the pure d⁸ configuration, U is the repulsive Coulomb energy between two 3d electrons on the same Ni site, and u is the attractive Coulomb energy between a 3d electron and an O 2p hole on nearest-neighbor sites. δE_B = E(d⁷ → d⁸p) ≈ ε_d - ε_p. Therefore δE_B is

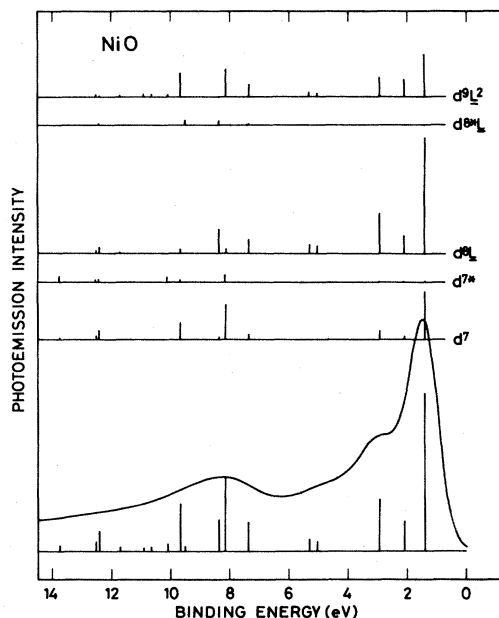


FIG. 2. Final-state components of the valence-band photoemission spectrum of NiO. d^{7*} denotes t_{2g}⁴e_g³ and t_{2g}³e_g⁴ configurations and d^{8*} denotes t_{2g}⁴e_g⁴ configurations, which result from configuration interactions within the d⁷ and d⁸ manifolds, respectively. Note the predominant d⁸L character in the main lines (0-4 eV).

lower than δE_A by $U-u$ which would be in the range of 5–10 eV.⁵⁷ (Note that the present definition of U includes solid-state relaxation effects involving ligand-Ni 4s, 4p interatomic polarization and is considerably reduced from the free-ion value (~ 27 eV) but does not fully include relaxation due to intra-atomic polarization of surrounding atoms.⁵⁸) In fact, δE_B was obtained to be -3.5 eV, which is lower than δE_A by 7 eV. Such a large difference between δE_A and δE_B was necessary in order to reproduce the intensity of the satellite. That is, this magnitude of U was necessary in order to explain the observed satellite intensity. $\delta E_C = E(d^8p \rightarrow d^9p^2)$ may be estimated as $\delta E_C \simeq \epsilon_d - \epsilon_p + U + U' - 2u$, where U' is the Coulomb repulsion between two O 2p holes and would be of the order of 1–2 eV if the two-hole correlation is ignored. We do not know exactly the value of u , since this Coulomb energy would be considerably reduced from a bare point-charge estimation (6.8 eV for NiO) by intra-atomic and interatomic polarization.⁵⁷ Thus δE_C would be lower than δE_A by a few eV, and therefore the value obtained here $\delta E_C = 1$ eV appears reasonable.

The valence-band spectrum of NiCl₂ was also calculated by the same procedure. Main differences from NiO are that the Cl is more electropositive than O and that the Ni 3d–Cl 2s, 2p overlaps are smaller than Ni 3d–O 2s, 2p ones. The smaller electronegativity of Cl leads to lowering of δE_A , δE_B , and δE_C with respect to those of NiO, while the smaller overlaps result in reduced Ni-Cl transfer and overlap integrals. The smaller orbital overlaps in NiCl₂ than in NiO are inferred from the smaller crystal-field parameter of the Ni²⁺ ion in spite of the smaller Ni 3d-ligand energy difference in NaCl (Ref. 64) than in MgO.^{40,65,66} In Fig. 3 the calculated spectrum is compared with the observed XPS spectrum of NiCl₂ (Ref. 26). The transfer and overlap integrals have been multiplied by a factor $f=0.95$ from the values in Ref. 1 or reduced by a factor of ~ 0.8 with respect to the values determined here for NiO. This reduction is consistent with the reduction of the crystal-field parameter from NiO or MgO:Ni²⁺ to NaCl:Ni²⁺ obtained from the $d \rightarrow d$ optical-absorption spectra as will be described in Sec. V. This also leads to a reduction of the main-satellite separation from NiO (~ 7 eV) to NiCl₂ (5–6 eV). In addition to the differences between NiO and NiCl₂ mentioned above, emission from the ligand Cl 3p levels should be stronger than that from O 2p in NiO due to the doubled number of the ligand atoms and the larger photoionization cross section of Cl 3p.⁶⁷ After superposition of the Cl 3p emission, the experimental spectrum is well reproduced as in Fig. 3. The calculated emission feature around 12 eV is absent in the XPS spectrum and in nonresonant ultraviolet photoemission spectra,²⁷ but this absence would probably be due to an artifact of the background subtraction, since it is clearly seen in the recent resonant photoemission data.³³ The values of δE_A , δE_B , and δE_C which were determined to give the best result (Table III) are in accordance with the above-mentioned differences between NiO and NiCl₂. Figure 3 shows that, unlike the XPS spectrum of NiO, most of the intensity of the main band is derived from the Cl 3p levels rather than the Ni 3d levels. The XPS valence bands of Cu dihalides,^{34,35} where d^8 satellites are

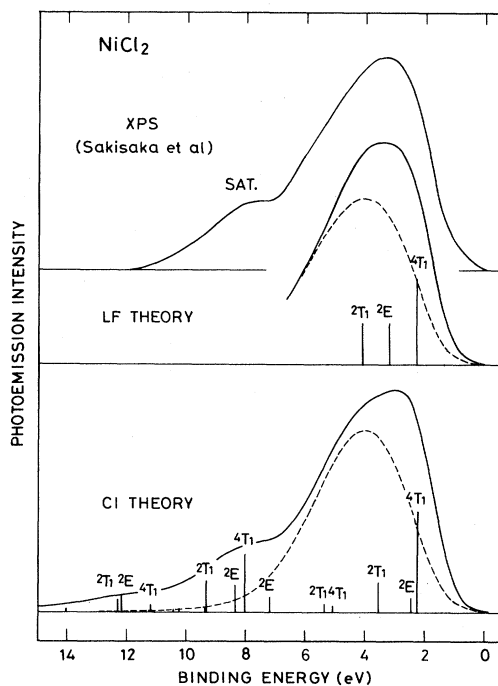


FIG. 3. Valence-band photoemission spectrum of NiCl₂ calculated by the configuration-interaction (CI) theory. The top panel shows the experimental XPS spectrum from Ref. 26. Multiplet of the d^7 final state calculated by the ligand-field (LF) theory ($B=0.09$ eV, $C=0.42$ eV, and $\Delta_{CF}=1.13$ eV) are also indicated. The dashed line shows emission from the Cl 3p band. The background has been subtracted already in the experimental spectrum (Ref. 26). For parameters used in the calculation, see Table III and text.

weak as compared to the d^9L main band, may also be interpreted in a similar manner.

We have used the experimental free-ion (Ni²⁺ and Ni³⁺ for the initial and final states, respectively) values for the Racah parameters B and C without empirical adjustment usually employed in the ligand-field theory when fitting $d \rightarrow d$ optical-absorption spectra^{7-9,40,41,53} and valence-band photoemission spectra.^{25-27,62} While the ligand-field theory requires the reduction of B and C by more than 30%, according to the configuration-interaction approach this apparent reduction of B and C is a direct consequence of the term-dependent energy shifts resulting from the configuration mixing. In the ligand-field theoretical fit of photoemission spectra of 3d transition-metal oxides,⁶² FeO, CoO, and NiO, the largest reduction of B and C has been found for NiO, which indicates that the configuration interactions in the final states or the mixing of ligand-hole states into d -hole states are the most significant in Ni compounds.

IV. RESONANT PHOTOEMISSION

The resonant behaviors of the valence-band spectra of Ni compounds at the 3p-core excitation threshold can be calculated as done by Davis and Feldkamp.⁶⁸ Exact treat-

ment of the resonant photoemission involving multiplet structures is, however, considerably complicated, and here we make a simplification in order to see qualitative behaviors. The initial state (1) with the 2×2 Hamiltonian (2) is used neglecting the multiplet structure of the $3d^n$ ion and the degeneracy of the ligand orbitals. Intermediate (discrete) states produced by the $3p \rightarrow 3d$ photoabsorption are given in the same manner as the initial and final (continuum) states by

$$\Psi_m = d_{m0} | \underline{c} d^9 \rangle + d_{m1} | \underline{c} d^{10} \underline{L} \rangle, \quad (13)$$

where \underline{c} denotes a core hole in the $3p$ shell, and the Hamiltonian is of the form

$$\tilde{H} = \begin{bmatrix} E'_0 & v''' \\ v''' & E'_0 + \delta E_D \end{bmatrix}. \quad (14)$$

The final state (4) is rewritten in order to show explicitly the continuum character as

$$\Psi_{fE} = b_{f0} | d^7 \epsilon f \rangle + b_{f1} | d^8 \underline{L} \epsilon f \rangle + b_{f2} | d^9 \underline{L}^2 \epsilon f \rangle, \quad (15)$$

where ϵf represents a photoemitted electron which is known to have mainly f character, and E is the energy of the cluster plus the photoemitted electron. Unit matrices were assumed for \tilde{S} .

The amplitude for photoemission producing a final state Ψ_{fE} is given by⁶⁸

$$D_f(E) = -\pi \sum_v \frac{[\pi / \Gamma_v(E)] [\pi q_v(E) + i]}{[z_v(E) + i\pi] \pi V_{f'v}(E)} \times \left[\sum_{f'} V_{f'v}(E) \langle \Psi_{f'E} | T | \Psi_g \rangle \right] - \pi \langle \Psi_{fE} | T | \Psi_g \rangle, \quad (16)$$

where

$$q_v(E) = \sum_m \frac{A_m^v(E) \langle \Psi_g | T | \Psi_m \rangle}{\pi \sum_{f'} V_{f'v}(E) \langle \Psi_g | T | \Psi_{f'E} \rangle}, \quad (17)$$

$$\Gamma_v(E) = \pi \sum_f V_{fv}(E) V_{fv}(E), \quad (18)$$

$$V_{fv}(E) = \sum_m A_m^v(E) V_{fm}, \quad (19)$$

and $z_v(E)$ and $A_m^v(E)$ are obtained by solving

$$\sum_m [(E_m - E) \delta_{mn} + (z_v(E) / \pi) \Gamma_{mn}] A_{mv}(E) = 0, \quad (20)$$

with

$$\Gamma_{mn} = \pi \sum_f V_{fm} V_{fn}. \quad (21)$$

Here, V_{fm} 's are super-Coster-Kronig matrix elements between discrete states Ψ_m and continuum states Ψ_{fE} and are given as linear combinations of $\langle d^7 \epsilon f | (e^2/r) | \underline{c} d^9 \rangle$ and $\langle d^8 \underline{L} \epsilon f | (e^2/r) | \underline{c} d^{10} \underline{L} \rangle$. $\langle \Psi_g | T | \Psi_{fE} \rangle$ and $\langle \Psi_g | T | \Psi_m \rangle$ are transition-matrix elements for the

$3d \rightarrow \epsilon f$ and $3p \rightarrow 3d$ transitions, and are linear combinations of $\langle d^8 | T | d^7 \epsilon f \rangle$ and $\langle d^9 \underline{L} | T | d^8 \underline{L} \epsilon f \rangle$, and those of $\langle d^8 | T | \underline{c} d^9 \rangle$ and $\langle d^9 \underline{L} | T | \underline{c} d^{10} \underline{L} \rangle$, respectively.

The values of δE_A , δE_B , and δE_C for NiO were chosen to be 5, -2, and 1 eV, respectively, rather than the values obtained in Sec. III in order to approximately take into account energy shifts due to multiplet splittings [e.g., $\Delta(^3A_2)$ in Eq. (9)] which have been omitted in this section. For the nondiagonal matrix elements of the Hamiltonian, $\langle d^8 | \tilde{H} | d^9 \underline{L} \rangle = 3.5$ eV was used.⁶⁹ Equation (16) was calculated for various values of the parameters $\langle d^8 | T | \underline{c} d^9 \rangle / \langle d^8 | T | d^7 \epsilon f \rangle$, $\langle d^7 \epsilon f | (e^2/r) | \underline{c} d^9 \rangle$, and $\delta E_D = E(\underline{c} d^9 \rightarrow \underline{c} d^{10} \underline{L})$. The experimental results that the main lines show a resonance dip and that the satellites that show resonance enhancement were reproduced with $\langle d^8 | T | \underline{c} d^9 \rangle / \langle d^8 | T | d^7 \epsilon f \rangle = 0.4$ eV, $\langle d^7 \epsilon f | (e^2/r) | \underline{c} d^9 \rangle = 0.7$ eV, and $\delta E_D = 6$ eV as is shown in Fig. 4(a). The experimental resonance profiles show additional features arising from the multiplet splitting of the intermediate $3p$ -hole state (predominantly $3p^5 3d^9$ -like) which is not included in the present model.

The resonant photoemission of NiCl₂ has shown more clearly enhancement of the satellite and dip of the main lines.³³ This is explained in the present model with use of parameters appropriate to NiCl₂, namely, lower δE_A , δE_B , δE_C , and δE_D ($\delta E_A = 3.5$ eV, $\delta E_B = -2.5$ eV, $\delta E_C = 0.5$ eV, and $\delta E_D = 5$ eV), and smaller $\langle d^8 | \tilde{H} | d^9 \underline{L} \rangle$ (= 3 eV), the result being shown in Fig. 4(b).

The stronger enhancement of the satellites rather than the main lines is partly due to the fact that, as can be seen in Fig. 2, the main lines contain more $d^8 \underline{L}$ final-state character which does not resonate. The large $d^8 \underline{L}$ weight in the main lines is due to the shake-down nature of the

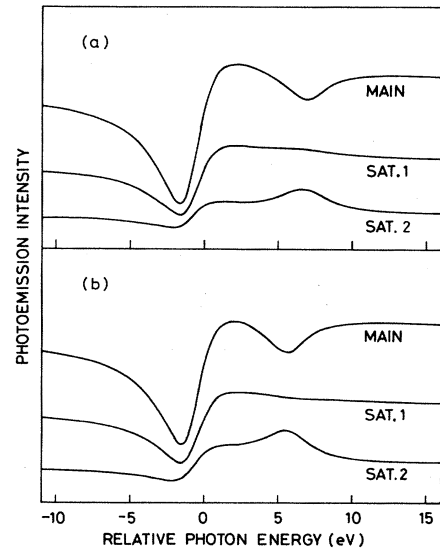


FIG. 4. Intensity profiles of photoemission lines calculated using parameters relevant to (a) NiO and (b) NiCl₂. The two satellite lines (denoted by sat. 1 and sat. 2) are calculated to be, respectively, (a) 7.2 and 10.7 eV, and (b) 7.6 and 9.4 eV below the main line. The 0 of photon energies corresponds to the excitation energy from the ground state to the $\underline{c} d^9$ state, where \underline{c} denotes a core hole in the Ni $3p$ shell.

valence-band satellite structure or equivalently due to the negative $\delta E_B = E(d^7 \rightarrow d^8 \underline{L})$. In order to see this clearly, resonant profiles were calculated with higher δE_A , δE_B , and δE_C (i.e., δE_B being smaller in magnitude), and in fact the satellite enhancement was reduced and the main line became more enhanced [Fig. 5(a)]. The higher δE_A , δE_B , and δE_C correspond to larger ionicity as is encountered in going from compounds of Ni to Co to Fe to Mn, and may explain the resonance behaviors of Ni, Co, Fe, and Mn dichlorides.³³ On the other hand, in the same series the number of $3d$ holes increases, which would result in an increased $3p \rightarrow 3d$ absorption intensity and a reduced $3d \rightarrow \epsilon f$ direct-emission intensity. In order to see this effect, intensity profiles were calculated for the d^6 (Fe^{2+}) case with the same δE_A , δE_B , and δE_C as in Fig. 4(a). The result is shown in Fig. 5(b), where one can see a pronounced variance from the d^8 case, Figs. 4 and 5(a). In fact, strong enhancement of the main lines rather than the satellite lines as in Fig. 5(b) has been found for the spectra of MnCl_2 and FeCl_2 .³³ We may thus conclude that the different resonance behaviors of the satellite structures in the $3d$ transition-metal dichlorides³³ are partly due to different degrees of covalency and partly and more importantly due to different $3p \rightarrow 3d$ and

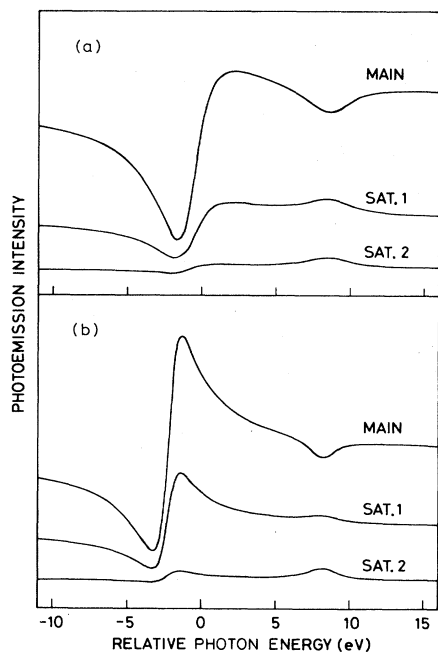


FIG. 5. Intensity profiles of photoemission lines calculated (a) using parameters relevant to NiO except that higher values are used for the $L \rightarrow d$ excitation energies ($\delta E_A = 7$ eV, $\delta E_B = 0$ eV, $\delta E_C = 3$ eV, and $\delta E_D = 8$ eV) and (b) those calculated using parameters relevant to NiO except that the electron number in the cluster is smaller by two corresponding to Fe^{2+} compounds. In calculating the profiles of (b), $\langle d^6 | T | d^5 \epsilon f \rangle = 0.67$ eV, $\langle d^6 | \tilde{H} | d^7 \underline{L} \rangle = 4.9$ eV, and $\langle d^4 \epsilon f | (e^2/r) \underline{d}^6 \rangle = 0.53$ eV have been used corresponding to the small number of electrons. The two satellite lines (denoted by sat. 1 and sat. 2) are calculated to be, respectively, (a) 7.9 and 11.0 eV, and (b) 8.8 and 14.0 eV below the main line.

$3d \rightarrow \epsilon f$ transition probabilities resulting from the different d -electron numbers.

V. INTRA-ATOMIC $d \rightarrow d$ OPTICAL ABSORPTION

Optical-absorption spectra due to intra-atomic $d \rightarrow d$ transitions in $3d$ transition-metal complexes are characterized by the crystal-field parameter Δ_{CF} and the reduced B and C parameters relative to the free-ion values. Molecular-orbital calculations¹⁰⁻¹² have demonstrated that both of these effects are due to covalent mixing between the $3d$ and ligand orbitals. According to the molecular-orbital theory, orbitals consisting the incomplete $3d$ shell are antibonding combinations of the $3d$ and ligand orbitals. In octahedrally coordinated $3d$ ions, the e_g level lies above the t_{2g} level by Δ_{CF} , because the overlap is greater between the $3d e_{2g}$ and ligand p_σ orbitals than between the $3d t_{2g}$ and p_π orbitals. Reduction of the B and C parameters are explained by reduction of the $3d$ component in the antibonding orbitals relative to the pure $3d$ orbitals.

In the configuration-interaction approach, the crystal-field parameter is defined as the total-energy difference between the ${}^3A_{2g}$ and ${}^3T_{2g}$ states, i.e., $\Delta_{\text{CF}} = E({}^3T_{2g}) - E({}^3A_{2g})$, since both terms contain the same combination of B and C .⁵³ The energies of other excited states with d^8 configuration (${}^1T_{1g}$, ${}^3T_{1g}$, ${}^3T_{2g}$, ${}^1T_{2g}$, 1E_g , and ${}^1A_{1g}$) can also be calculated by the configuration-interaction theory. The wave function and Hamiltonian for each term have the same form as Eqs. (8) and (9) except that, in cases where p_π -hole states are allowed, the size of the matrix (9) becomes larger. In Table IV the basis functions and the Hamiltonian for each symmetry are listed. The lowest one or two energy levels of each symmetry are mainly d^8 -like, and the so-called $d \rightarrow d$ transitions occur from the ${}^3A_{2g}$ ground state into these levels. This situation is schematically shown in the energy-level diagram of the NiO_6^{10} cluster in Fig. 6. Optical absorption due to charge-transfer transitions is also shown in the figure and will be discussed in Sec. VI.

In Fig. 7, the optical-absorption spectrum of NiO by Newman and Chrenko⁴¹ in the energy range below ~ 4 eV is compared with the calculated-energy levels. In the ligand-field theory, there are three adjustable parameters, Δ_{CF} , B , and C , in calculating $d \rightarrow d$ transition energies, whereas we have two parameters, δE_A and the scaling factor f , for the transfer and overlap integrals. Both parameters have been determined in the fit of the photoemission spectrum in Sec. III and are given in Table III, but these gave only about half of the observed Δ_{CF} . Then f was varied in order to make Δ_{CF} in agreement with experiment or in order to obtain a correct energy for the lowest ${}^3T_{2g}$ level. As the calculated energy levels were not sensitive to δE_A , we fixed δE_A at the value in Table III. Energy levels calculated with $f = 1.6$ instead of $f = 1.13$ in Table III (designated by "CI theory" in Fig. 7) show good correspondence to the experiment. In the figure, energy levels obtained using the Tanabe-Sugano diagram⁵³ with $B = 0.115$ eV, $\Delta_{\text{CF}} = 1.13$ eV, and $B/C = 4.71$ are also shown (denoted by "LF theory"). Both of the theoretical energy levels show comparable agreement with experi-

TABLE IV. Basis functions and Hamiltonians for the NiO_6^{10-} (NiCl_6^{4-}) cluster, which give the ground state and final states of intraatomic $d \rightarrow d$ optical transitions. The symmetry of p_σ , p_π , and p_ξ is 2E_g , ${}^2T_{2g}$, and 2E_g , respectively. The overlap matrices are obtained as in Table I. $K = E_8 = (43 + \frac{5}{9})B - (21 + \frac{7}{9})C$; $L = E_8 + \delta E_A$; $L' = L + \epsilon_p - \epsilon_s$.

(a) ${}^3A_{2g}$ symmetry
$\varphi_1 = t_2^6 e^{23} A_2\rangle$, $\varphi_2 = t_2^6 e^3 p_\sigma^3 A_2\rangle$, $\varphi_3 = t_2^6 e^3 p_\xi^3 A_2\rangle$ $H_{1,1} = K - 50B + 21C$, $H_{2,2} = L$, $H_{3,3} = L'$ $H_{1,2} = \sqrt{2}v_\sigma$, $H_{1,3} = \sqrt{2}v_s$
(b) ${}^3T_{2g}$ symmetry
$\varphi_1 = t_2^5 e^{33} T_2\rangle$, $\varphi_2 = t_2^5 e^4 p_\sigma^3 T_2\rangle$, $\varphi_3 = t_2^6 e^3 p_\pi^3 T_2\rangle$ $\varphi_4 = t_2^5 e^4 p_\xi^3 T_2\rangle$ $H_{1,1} = K - 50B + 21C + \Delta$, $H_{2,2} = L + \Delta$, $H_{3,3} = L - \delta$ $H_{4,4} = L' + \Delta$, $H_{1,2} = v_\sigma$, $H_{1,3} = v_\pi$ $H_{1,4} = v_s$
(c) ${}^1T_{1g}$ symmetry
$\varphi_1 = t_2^5 e^{31} T_1\rangle$, $\varphi_2 = t_2^5 e^4 p_\sigma^1 T_1\rangle$, $\varphi_3 = t_2^6 e^3 p_\pi^1 T_1\rangle$ $\varphi_4 = t_2^5 e^4 p_\xi^1 T_1\rangle$ $H_{1,1} = K - 38B + 23C + \Delta$, $H_{2,2} = L + \Delta$, $H_{3,3} = L - \delta$ $H_{4,4} = L' + \Delta$, $H_{1,2} = v_\sigma$, $H_{1,3} = v_\pi$ $H_{1,4} = v_s$
(d) ${}^3T_{1g}$ symmetry
$\varphi_1 = t_2^4 e^{33} T_1\rangle$, $\varphi_2 = t_2^4 e^{43} T_1\rangle$, $\varphi_3 = t_2^5 e^4 p_\sigma^3 T_1\rangle$ $\varphi_4 = t_2^6 e^3 p_\pi^3 T_1\rangle$, $\varphi_5 = t_2^5 e^4 p_\pi^3 T_1\rangle$, $\varphi_6 = t_2^5 e^4 p_\xi^3 T_1\rangle$ $H_{1,1} = K - 38B + 21C + \Delta$, $H_{2,2} = K - 47B + 21C + 2\Delta$, $H_{3,3} = L + \Delta$ $H_{4,4} = L - \delta$, $H_{5,5} = L + \Delta - \delta$, $H_{6,6} = L' + \Delta$ $H_{1,2} = 6B$, $H_{1,3} = v_\sigma$, $H_{1,4} = v_\pi$ $H_{1,6} = v_s$, $H_{2,5} = \sqrt{2}v_\pi$
(e) ${}^1T_{2g}$ symmetry
$\varphi_1 = t_2^5 e^{31} T_2\rangle$, $\varphi_2 = t_2^4 e^{41} T_2\rangle$, $\varphi_3 = t_2^5 e^4 p_\sigma^1 T_2\rangle$ $\varphi_4 = t_2^6 e^3 p_\pi^1 T_2\rangle$, $\varphi_5 = t_2^5 e^4 p_\pi^1 T_2\rangle$, $\varphi_6 = t_2^5 e^4 p_\xi^1 T_2\rangle$ $H_{1,1} = K - 42B + 23C + \Delta$, $H_{2,2} = K - 41B + 23C + 2\Delta$, $H_{3,3} = L + \Delta$ $H_{4,4} = L - \delta$, $H_{5,5} = L + \Delta - \delta$, $H_{6,6} = L' + \Delta$ $H_{1,2} = 2\sqrt{3}B$, $H_{1,3} = v_\sigma$, $H_{1,4} = v_\pi$ $H_{1,6} = v_s$, $H_{2,5} = \sqrt{2}v_\pi$
(f) 1E_g symmetry
$\varphi_1 = t_2^6 e^{21} E\rangle$, $\varphi_2 = t_2^4 e^{41} E\rangle$, $\varphi_3 = t_2^6 e^3 p_\sigma^1 E\rangle$ $\varphi_4 = t_2^5 e^4 p_\pi^1 E\rangle$, $\varphi_5 = t_2^6 e^3 p_\xi^1 E\rangle$ $H_{1,1} = K - 42B + 23C$, $H_{2,2} = K - 41B + 23C + 2\Delta$, $H_{3,3} = L$ $H_{4,4} = L + \Delta - \delta$, $H_{5,5} = L'$, $H_{1,2} = -2\sqrt{3}B$ $H_{1,3} = \sqrt{2}v_\sigma$, $H_{1,5} = \sqrt{2}v_s$, $H_{2,4} = \sqrt{2}v_\pi$
(g) ${}^1A_{1g}$ symmetry
$\varphi_1 = t_2^6 e^{21} A_1\rangle$, $\varphi_2 = t_2^4 e^{41} A_1\rangle$, $\varphi_3 = t_2^6 e^3 p_\sigma^1 A_1\rangle$ $\varphi_4 = t_2^5 e^4 p_\pi^1 A_1\rangle$, $\varphi_5 = t_2^6 e^3 p_\xi^1 A_1\rangle$ $H_{1,1} = K - 34B + 25C$, $H_{2,2} = K - 32B + 26C + 2\Delta$, $H_{3,3} = L$ $H_{4,4} = L + \Delta - \delta$, $H_{5,5} = L'$, $H_{1,2} = \sqrt{6}(2B + C)$ $H_{1,3} = \sqrt{2}v_\sigma$, $H_{1,5} = \sqrt{2}v_s$, $H_{2,4} = \sqrt{2}v_\pi$

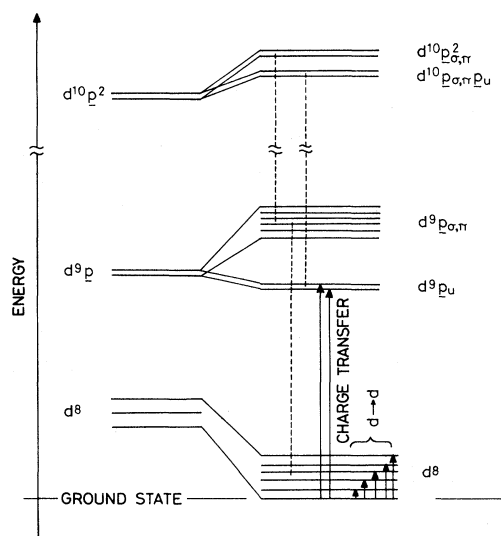


FIG. 6. Schematic energy-level diagram of the NiO₆⁻¹⁰ cluster. d^8 , d^9p_u , etc., denote predominant configuration components. Those configurations which interact strongly via Ni 3*d*-O 2*p* hybridization are connected by dashed lines. Charge-transfer $p \rightarrow d$ and intra-atomic $d \rightarrow d$ optical transitions are indicated by arrows. Excited states with O 2*s* hole(s) are not shown.

ment. The correspondence between the configuration-interaction theory and the experiment is excellent considering that only one parameter f has been adjusted by fitting one energy level ${}^3T_{2g}$. Note again that B and C used

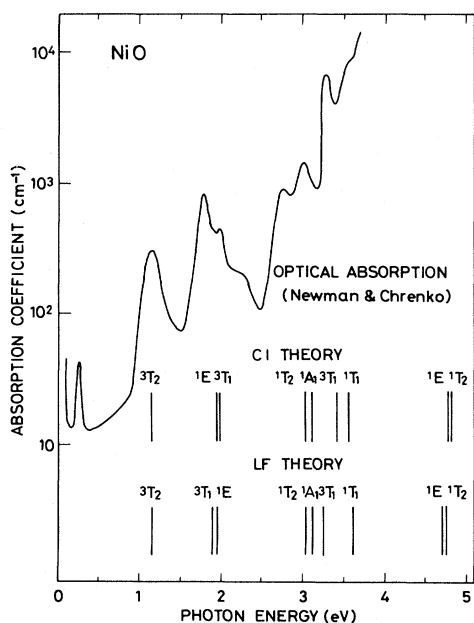


FIG. 7. Intra-atomic $d \rightarrow d$ optical transition energies for NiO calculated by the configuration-interaction (CI) theory compared with those calculated by the ligand-field (LF) theory. The optical-absorption spectrum by Newman and Chrenko (Ref. 41) is also shown. For parameters used in the calculation, see text.

in the configuration-interaction calculation are those of the free ion, while B and C in the ligand-field theory have been reduced by $\sim 10\%$ from the Ni²⁺ free-ion values. Thus the crystal-field splitting and the reduction of the B and C parameters are attributed to the same origin, namely, interactions between the d^8 and d^9L configurations. The difference in f between photoemission and optical absorption would be due to contraction of the 3*d* orbitals in the ionized photoemission final states.

Optical absorption of NiCl₂ due to $d \rightarrow d$ transitions has not been reported so far to the author's knowledge, but instead we may compare the spectra of NaCl:Ni²⁺ with the energy levels of the NiCl₆ cluster calculated using parameters appropriate to NiCl₂. It would be sensible to make such a comparison because an optical-absorption study^{65,66} on Mg_{1-x}Ni_xO, where the Ni-O distance changes little with composition x , has demonstrated the independence of the $d \rightarrow d$ transition energies on x and that the Ni-Cl distance differs by only 0.2 Å between NiCl₂ and NaCl:Ni²⁺. For NaCl:Ni²⁺, $\Delta_{CF}=0.84$ eV has been obtained.⁶⁴ Δ_{CF} of NiCl₂ calculated with use of the parameters in Table III ($f=0.95$) was again too small. Then the experimentally observed Δ_{CF} of NaCl:Ni²⁺ was reproduced by using a larger scaling factor $f=1.27$, which is larger than the photoemission value $f=0.95$ by a factor of ~ 1.3 . (For NiO, f for $d \rightarrow d$ transitions is larger than that in Table III by ~ 1.4 .)

VI. CHARGE-TRANSFER OPTICAL ABSORPTION

Optical-absorption features of NiO in the energy range between the fundamental absorption edge (~ 4 eV) and ~ 9 eV can be ascribed to transitions involving Ni 3*d* electrons,^{42,43} since they are absent in MgO, having a nearly identical lattice parameter to NiO,^{44,57} but it has not yet been well established what transitions are responsible for these structures. Particularly, the origin of the fundamental-absorption edge at ~ 4 eV has been the subject of much controversy. Two alternative possibilities have been proposed: one is O 2*p* \rightarrow Ni 3*d* charge-transfer transitions and the other is Ni 3*d* \rightarrow 4*s* intra-atomic transitions. In addition to these two, $d \rightarrow d$ charge transfer between neighboring Ni ions has also been proposed. Several arguments for the above assignment have been critically reviewed by Brandow.⁵⁷

In terms of the present configuration-interaction theory using parameters determined so far, we estimate energies for the charge-transfer transitions. In the cluster model, dipole-allowed $p \rightarrow d$ transitions should involve ligand p molecular orbitals with odd parity. In the case of the NiO₆ cluster, one t_{2u} and two t_{1u} orbitals are formed from the ligand p orbitals, and their one-electron orbital energies are given in terms of p - p transfer integrals ($pp\sigma$) and ($pp\pi$). The final states of the charge-transfer transitions are therefore to be given by

$$\begin{aligned} \Psi_f = & e_{f0} | t_2^6 e^3 ({}^2E) p_u \rangle \\ & + e_{f1} | t_2^6 e^4 p_\sigma ({}^2E) p_u \rangle \\ & + e_{f2} | t_2^6 e^4 p_\pi ({}^2E) p_u \rangle, \end{aligned} \quad (22)$$

with the first term ($d^9\bar{L}$ -like) predominant, where \bar{p}_u represents a t_{1u^-} or t_{2u^-} -like ligand p -hole. Transitions from the ground state (8) to the charge-transfer states (22) are schematically shown in Fig. 6. Note that (22) does not contain a mixture of the d^8 configuration because of its odd symmetry.

For NiCl_2 , by using the parameters determined for photoemission (Table III, $f=0.95$) and the Mattheiss's values¹ for ($pp\sigma$) and ($pp\pi$) for NiO (those for NiCl_2 have not been obtained but are expected to be similar to the NiO values), excitation energies from the ground state (8) to the first term in (22) $|t_2^6 e^3(^2E)\bar{p}_u\rangle$ were calculated to be 5.9, 6.5, and 7.2 eV corresponding, respectively, to t_{1u^-} , t_{2u^-} , and t_{1u^-} -like p_u holes. The two t_{1u^-} -hole states are expected to give stronger absorption than the t_{2u^-} one, since t_{1u^-} -like ligand orbitals mix with high-lying Ni $4p$ states, because of the same symmetry with respect to the Ni site, and that the p $t_{1u^-} \rightarrow d$ transitions involve intra-atomic $4p \rightarrow 3d$ matrix elements. With the use of $f=1.27$ determined for intra-atomic $d \rightarrow d$ excitations instead, values 7.2, 7.8, and 8.5 eV were obtained. (f for intra-atomic $d \rightarrow d$ transitions would be more appropriate in this case, because the number of electrons in the cluster is the same for the $d \rightarrow d$ and $p \rightarrow d$ optical absorption.) Experimentally, charge-transfer optical absorption has been observed as two peaks at ≤ 5 eV for NiCl_2 (Refs. 70 and 71) and at 5–6 eV in NaCl:Ni^{2+} (Ref. 72), probably corresponding to the two t_{1u^-} -like ligand holes. Thus the observed energies are lower than the calculated energy of $|t_2^6 e^3(^2E)\bar{p}_u\rangle$ by 2–3 eV as a whole due to hybridization with $|t_2^6 e^4 p_\sigma(^2E)\bar{p}_u\rangle$ and $|t_2^6 e^4 \bar{g}(^2E)\bar{p}_u\rangle$ and due to final-state relaxation that cannot be included in adjustable parameters. By using the parameters of NiO determined by photoemission with $f=1.13$ (determined for intra-atomic $d \rightarrow d$ transitions with $f=1.6$), excitation energies from the ground state to $|t_2^6 e^3(^2E)\bar{p}_u\rangle$ were calculated to be 7.7, 8.3, and 9.0 eV (9.6, 10.2, and 10.9 eV). Therefore, if effects of the hybridization and relaxation in the final states are assumed to be of the same order in NiO and NiCl_2 , then some of the features (probably two out of several peaks as in NiCl_2 and NaCl:Ni^{2+}) at least above 6–7 eV in the NiO spectrum⁴² should be assigned to $p \rightarrow d$ charge-transfer transitions, so that the energy of the fundamental absorption edge seems to be too low to be ascribed to $p \rightarrow d$ transitions. The recent optical study⁶⁵ of $\text{Mg}_{1-x}\text{Ni}_x\text{O}$ has also suggested that the $p \rightarrow d$ charge-transfer transitions occur above 6 eV.

Then the absorption edge at ~ 4 eV would be assigned either to the $3d \rightarrow 4s$ or interatomic $3d \rightarrow 3d$ charge-transfer transitions. Most of the researchers^{42–44} prefer the former, but we would argue against it for the following reasons. Firstly, one would expect $3d \rightarrow 4s$ transitions to occur nearly at the same energies in the dilute system $\text{Mg}_{1-x}\text{Ni}_x\text{O}$ since these transitions are almost intratomic, but these have not been observed.⁶⁵ Secondly, the $3d \rightarrow 4s$ transitions are atomically forbidden and, if this selection rule is relaxed in solids, would not account for the observed intensity around 4 eV. On the other hand, the interatomic $d \rightarrow d$ transition intensity would increase with increasing Ni concentration and would explain their absence in the dilute system. Generally one would expect

that the $d \rightarrow d$ transitions are weak because of the small direct overlaps between neighboring d orbitals. However, in the case of NiO, we have shown in Sec. III that d -hole states contain a large ligand p -hole component and therefore the $d \rightarrow d$ transitions would involve $p \rightarrow d$ dipole matrix elements. In this sense, it might not be very meaningful to distinguish strictly between the $p \rightarrow d$ and $d \rightarrow d$ processes, since both of these two processes involve more or less $p \rightarrow d$ charge transfer and differ mainly in the degree of localization of the excitations. Absence of absorption features that can be clearly identified as interatomic $d \rightarrow d$ transitions in CoO (Ref. 42) and MnO (Ref. 43) would be due to the smaller p -hole component in the d -hole state, thus the smaller $p \rightarrow d$ component in the transition-matrix elements. As for the energy positions, the lowest empty d states lies at ~ 4 eV (E_e in Fig. 8) above E_F as we shall see in the next section, and the highest occupied d state at ~ 1 eV (E_h in Fig. 8) below E_F . Thus the $d \rightarrow d$ excitation threshold becomes ~ 5 eV minus the screened nearest-neighbor Ni-Ni Coulomb energy and would fall in the range of the fundamental absorption edge. The $d \rightarrow d$ charge-transfer energy in NiCl_2 was estimated to be nearly identical to that in NiO or around the $p \rightarrow d$ charge-transfer region of NiCl_2 , but these features have not been clearly observed,⁷⁰ probably due to overlap with $p \rightarrow d$ absorption. The smaller number of Ni-Ni nearest-neighbor pairs in the NiCl_2 crystal structure than in NiO may make the $d \rightarrow d$ intensity low.

A recent band calculation of NiO (Ref. 73) has attributed to 4-eV edge to $p \rightarrow d$ transitions based on the calculated interband optical-absorption coefficient. However, we note that there has been large ambiguity in the calculated Ni $3d$ –O $2p$ energy separation, even if calculations are carried out to self-consistency.^{2,4–6} Moreover, one-

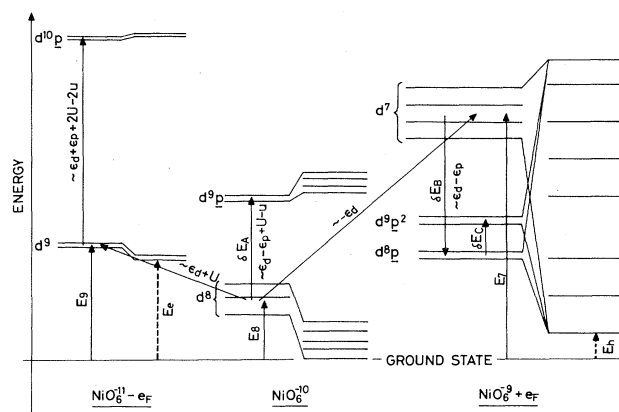


FIG. 8. Schematic energy-level diagrams of the NiO_6^{-10} cluster, which represents the ground state, intra-atomic $d \rightarrow d$ excited states, and $p \rightarrow d$ charge-transfer states, the NiO_6^{-9} cluster, which represents final states of valence-band photoemission, and the NiO_6^{-11} cluster, which represents final states of isochromat spectroscopy. Energies E_7 , E_8 , δE_A , δE_B , etc., are defined in the text. E_e and E_h are the minimum energies required to create an electron and a hole, respectively, from the NiO_6^{-10} -cluster ground state. e_F denotes an electron at E_F .

electron energies obtained by band calculations may not be relevant to localized excitations such as the $p \rightarrow d$ excitations. The calculated $p \rightarrow d$ peak in the absorption coefficient⁷³ is concentrated in a narrow intense peak around ~ 4 eV, while the experiment⁴² has shown absorption in a wide energy range of 4–9 eV. This discrepancy would be attributed to a spread of the $p \rightarrow d$ oscillator strength into the wide energy range due to the localized interactions considered in this section which have not been taken into account in the one-electron energy-band picture. We have considered so far localized excitations as a possible origin of the structures at ≥ 4 eV. A photoconductivity measurement,⁷⁴ on the other hand, has given a gap of $\lesssim 4$ eV, which suggests creation of delocalized electrons and/or holes. However, reliable electrical measurements have been hindered by high resistivity, surface conductivity, sample imperfection, etc.,⁷⁵ and we cannot safely base the assignment of optical spectra on these results.

VII. ISOCHROMAT SPECTRA

While photoemission probes occupied energy levels, isochromat spectroscopy gives information about unoccupied levels. So far, the isochromat spectrum of NiO have been reported only for oxidized Ni(100) surfaces⁴⁵ where a thin NiO layer is formed. In their results, a prominent peak has been observed at about 4 eV above E_F . In addition to this peak, a very weak shoulder has been observed at 1 eV above E_F , which these authors identified as empty 3*d* states. This assignment, however, seems to be incompatible with the strong *d*-peak intensity observed for the isochromat spectrum Ni metal reported by the same authors.

The final states of isochromat spectroscopy, Eq. (7), after the transition of an incident electron into an empty *d* level, are more explicitly written as

$$\begin{aligned} \Psi_f = & c_{f0} |t_2^6 e^3 ({}^2E)\rangle + c_{f1} |t_2^6 e^4 \underline{p}_\sigma ({}^2E)\rangle \\ & + c_{f2} |t_2^6 e^4 \underline{d} ({}^2E)\rangle. \end{aligned} \quad (23)$$

The main *d* feature in the isochromat spectrum would be mostly d^9 -like represented by the first term of (23). The energy of the d^9 final state $|t_2^6 e^3 ({}^2E)\rangle$ measured from the ground state of the cluster plus an electron at E_F , E_9 , is calculated as follows. E_8 is calculated to be 4.6 eV above the ground state with use of the parameters in Table III which have been determined for photoemission ($f = 1.13$). $E_9 - E_8 \simeq \epsilon_d + U$, where $-\epsilon_d \simeq E_7 - E_8 = 9.0$ eV and $U \simeq \delta E_A - \delta E_B + u = 7.5 + u$. Thus $E_9 = (E_9 - E_8) + E_8 \simeq 3.1 + u = 4 - 5$ eV. If we use $f = 1.6$ determined for the intra-atomic $d \rightarrow d$ transitions, E_8 is calculated to be 6.5 eV, so that $E_9 = 6 - 7$ eV. The latter values are expected to be more appropriate for the same reason as for the $p \rightarrow d$ transitions in Sec. VI. Hybridization between the d^9 and $d^{10}\underline{L}$ states and relaxation in the final state would make the energy of (23) lower than E_9 by at most 2–3 eV. The energies thus derived are those for isochromat spectra with the same reference level as that of the photoemission spectra of Ref. 31 which have been corrected for charging effects. Charging effects are expected to be small for the oxide layer of Ref. 45. After correcting charging effects, there could still be in principle uncertainty of the band-gap energy in the reference levels for

different samples, but both the single-crystal NiO (Ref. 31) and the oxide layer⁴⁵ are expected to be *p*-type so that E_F would not vary so much between them. If we assume the reference level E_F is the same for the single crystal and the oxide layer, the present result suggests that the weak feature of ~ 1 eV above E_F cannot be due to transitions into *d* states but that the intense peak at ~ 4 eV above E_F is due to empty *d* states. For more unambiguous identification of the isochromat spectrum, isochromat and photoemission experiments should be performed on the same sample which is not affected by charging effects, e.g., thin oxide layers on Ni metal.

VIII. DISCUSSION

We have studied photoemission, inverse photoemission, optical-absorption, and isochromat spectra of insulating Ni compounds, so-called Mott insulators, using the cluster model with strong correlation of 3*d* electrons. It has been implicitly assumed that the electronic states of both the ground and excited states are localized within the cluster. This assumption may not be correct especially for the excited states, since the excitation could move in the crystal with appropriate effective transfer integrals. In the case of intra-atomic $d \rightarrow d$ optical transitions, the transfer integrals are negligibly small (< 0.1 eV), because two particles (an electron and a hole) must be transferred simultaneously.⁵⁷ On the other hand, one would expect that an isolated hole produced by photoemission moves with transfer integrals of the order of the bandwidths obtained in the antiferromagnetic band-structure calculations^{3–6} (~ 1 eV) and that the photoemission lines show these bandwidths. However, the main lines of NiO are narrow and seem to exhibit widths only of instrumental and lifetime broadening. This would be explained by the dominant $d^8\underline{L}$ character in these final-state lines: The *d* hole is accompanied by ligand $\rightarrow d$ charge transfer and therefore three particles, the photo-produced *d* hole, the *d* electron, and the ligand hole, the latter two being produced by the charge transfer, must be transferred from site to site. This is analogous to a polaron in ionic crystals, and corresponding transfer integrals would be considerably reduced from the one-electron values. This polaronic effect is also expected for the satellite lines, but the lifetime width in the satellite region is much larger than the one-electron band width.

In metallic Ni compounds [NiSb, NiTe (Ref. 32), NiS (Ref. 23)] and Ni metal, the satellites observed several eV below the main *d* band have been explained as two-hole bound states,^{46–51} while the main lines have been considered to be a delocalized hole in the Ni 3*d* band. This situation appears quite different from the case of insulators studied here. However, the similarity in the satellite features and their $3p \rightarrow 3d$ resonance profiles between the insulating and metallic Ni compounds³² suggests that similar multielectron processes are taking place in these systems. Davis and Feldkamp⁵⁰ has shown that a *d* hole produced in the majority-spin band is screened by minority-spin *d* electrons transferred to the hole site. This may be related to the ligand $\rightarrow d$ charge-transfer screening mechanism studied in the present work. Our re-

sults thus might suggest that for Ni metal not only $d \rightarrow d$ screening considered so far⁴⁸⁻⁵⁰ but also Ni $4s, 4p \rightarrow Ni 3d$ screening must be taken into account in order to treat quantitatively the valence-band spectra of Ni. Importance of the sp screening for the d hole in Ni has already been pointed out by Kanamori,⁷⁶ who has suggested that not only electron correlation within the d band but also screening by sp electrons is responsible for the narrowing of the Ni main d band.

Conversely, it could be possible that effects of the nearest-neighbor $d-d$ interactions influence the spectra of the insulating Ni compounds. It has been shown that, even for electrons in a wide band, energies of photoemission final states are better approximated by those of localized holes screened by electronic polarization rather than by those of extended holes.⁷⁷ So the present calculations of photoemission spectra using the cluster model which

neglects interatomic $d-d$ interactions would be a good approximation for the Ni compounds, in spite of the fact that the bandwidth of Ni $3d$ is a few times larger than the previously studied Ce compounds.³⁹ However, the intensities of isochromat spectra of Ce compounds could not be explained quantitatively by single-Ce-ion models,⁷⁸ which might be attributed to the neglect of Ce $4f$ -Ce $4f$ interactions.⁷⁹ In this respect, inclusion of interatomic $d-d$ interactions or equivalently itinerant character of d electrons and holes might somewhat modify our calculated spectral intensities. This problem remains to be studied.

ACKNOWLEDGMENTS

We would like to thank Professor S. Sugano, Professor T. Ishii, Professor S. Suga, Dr. T. Chiba, and Professor K. Terakura for valuable discussions.

*Temporary address: Department of Chemical Engineering and Materials Science, University of Minnesota, Minneapolis, MN 55455.

¹L. F. Mattheiss, *Phys. Rev. B* **5**, 290 (1972).

²A. B. Kunz and G. T. Surratt, *Solid State Commun.* **25**, 9 (1978).

³T. M. Wilson, *Int. J. Quant. Chem. Symp.* **2**, 269 (1968); **3**, 757 (1970).

⁴A. B. Kunz, *J. Phys. C* **14**, L455 (1981).

⁵K. Terakura, A. R. Williams, T. Oguchi, and J. Kübler, *Phys. Rev. Lett.* **52**, 1830 (1984); T. Oguchi, K. Terakura, and A. R. Williams, *Phys. Rev. B* **28**, 6443 (1983).

⁶J. Yamashita and S. Asano, *J. Phys. Soc. Jpn.* **52**, 3514 (1983).

⁷S. Sugano, Y. Tanabe and H. Kamimura, *Multiplets of Transition-Metal Ions in Crystals* (Academic, New York, 1970).

⁸J. S. Griffith, *The Theory of Transition-Metal Ions* (Cambridge University, Cambridge, 1961).

⁹C. K. Jørgensen, *Modern Aspects of Ligand-Field Theory* (North-Holland, Amsterdam, 1971).

¹⁰S. Sugano and R. G. Schulman, *Phys. Rev.* **130**, 517 (1963).

¹¹R. E. Watson and A. J. Freeman, *Phys. Rev.* **134**, A1526 (1964).

¹²E. Šimánek and Z. Šroubek, *Phys. Status Solidi* **4**, 251 (1964).

¹³M. Tinkham, *Proc. R. Soc. London, Ser. A* **236**, 535 (1956).

¹⁴R. G. Shulman and K. Knox, *Phys. Rev. Lett.* **4**, 603 (1960).

¹⁵R. G. Shulman and S. Sugano, *Phys. Rev.* **130**, 506 (1963).

¹⁶J. H. Hubbard and W. Marshall, *Proc. Phys. Soc. London* **86**, 561 (1965).

¹⁷B. E. F. Fender, A. J. Jacobson, and F. A. Wedgewood, *J. Chem. Phys.* **48**, 990 (1968).

¹⁸T. Chiba and N. Tsuda, *Appl. Phys.* **5**, 37 (1974).

¹⁹M. Cardona and L. Ley, *Photoemission in Solids I* (Springer, Berlin, 1978).

²⁰G. Wendin, *Structure and Bonding* (Springer, Berlin, 1981), Vol. 45.

²¹G. K. Wertheim and S. Hüfner, *Phys. Rev. Lett.* **2**, 1028 (1972).

²²G. K. Wertheim, H. J. Guggenheim, and S. Hüfner, *Phys. Rev. Lett.* **30**, 1050 (1973).

²³S. Hüfner and G. K. Wertheim, *Phys. Rev. B* **8**, 4857 (1973).

²⁴K. S. Kim, *Chem. Phys. Lett.* **26**, 234 (1974).

²⁵D. E. Eastman and J. L. Freeouf, *Phys. Rev. Lett.* **34**, 395

(1975).

²⁶Y. Sakisaka, T. Ishii, and T. Sagawa, *J. Phys. Jpn.* **36**, 1372 (1974).

²⁷T. Ishii, S. Kono, S. Suzuki, I. Nagakura, T. Sagawa, R. Kato, M. Watanabe, and S. Sato, *Phys. Rev. B* **12**, 4320 (1975).

²⁸S. Asada and S. Sugano, *J. Phys. Soc. Jpn.* **41**, 1291 (1976).

²⁹S. Larsson, *Chem. Phys. Lett.* **32**, 401 (1975); **40**, 362 (1976); S. Larsson and M. Braga, *ibid.* **48**, 596 (1977).

³⁰K. S. Kim, *J. Electron Spectrosc. Relat. Phenom.* **3**, 217 (1974).

³¹M. R. Thuler, R. L. Bendow, and Z. Hurych, *Phys. Rev. B* **27**, 2082 (1983).

³²S.-J. Oh, J. W. Allen, I. Lindau, and J. C. Mikkelsen, Jr., *Phys. Rev. B* **26**, 4845 (1982).

³³A. Kakizaki, K. Sugeno, T. Ishii, H. Sugawara, I. Nagakura, and S. Shin, *Phys. Rev. B* **28**, 1026 (1983).

³⁴L. C. Davis, *Phys. Rev. B* **25**, 2912 (1982).

³⁵G. van der Laan, C. Westra, C. Haas, and G. A. Sawatzky, *Phys. Rev. B* **23**, 4369 (1981).

³⁶G. van der Laan, *Solid State Commun.* **42**, 165 (1982).

³⁷M. R. Thuler, R. L. Benbow, and Z. Hurych, *Phys. Rev. B* **26**, 669 (1982).

³⁸J. Hubbard, D. E. Rimmer, and F. R. A. Hopgood, *Proc. Phys. Soc. London* **88**, 13 (1966).

³⁹A. Fujimori, *Phys. Rev. B* **27**, 3992 (1983); **28**, 2281 (1983); **28**, 4489 (1983).

⁴⁰W. Low, *Phys. Rev.* **109**, 247 (1958).

⁴¹R. Newman and R. M. Chrenko, *Phys. Rev.* **114**, 1507 (1959).

⁴²R. J. Powell and W. E. Spicer, *Phys. Rev. B* **2**, 2182 (1970).

⁴³L. Messick, W. C. Walker, and R. Glosner, *Phys. Rev. B* **6**, 3941 (1972).

⁴⁴S. Suga, K. Inoue, M. Taniguchi, S. Shin, M. Seki, K. Sato, and T. Teranishi, *J. Phys. Soc. Jpn.* **52**, 1848 (1983).

⁴⁵H. Scheidt, M. Glöbel, and V. Dose, *Surf. Sci.* **112**, 97 (1981).

⁴⁶S. Hüfner and G. K. Wertheim, *Phys. Lett. A* **47**, 349 (1974).

⁴⁷C. Guillot, Y. Ballu, J. Paigné, J. Lecante, K. P. Jain, P. Thiry, R. Pinchaux, Y. Pétrouff, and L. M. Falicov, *Phys. Rev. Lett.* **39**, 1632 (1977).

⁴⁸D. R. Penn, *Phys. Rev. Lett.* **42**, 921 (1979).

⁴⁹A. Liebsch, *Phys. Rev. Lett.* **43**, 1431 (1979).

⁵⁰L. C. Davis and L. A. Feldkamp, *J. Appl. Phys.* **50**, 1944 (1979).

⁵¹N. Martensson and B. Johansson, *Phys. Rev. Lett.* **45**, 482

- (1980).
- ⁵²A. Fujimori, F. Minami, and S. Sugano, *Phys. Rev. B* **29**, 5225 (1984).
- ⁵³Y. Tanabe and S. Sugano, *J. Phys. Soc. Jpn.* **9**, 753 (1954); **9**, 767 (1954).
- ⁵⁴T. Chiba and T. Akahane (unpublished).
- ⁵⁵N. H. Sabelli, *J. Chem. Phys.* **76**, 2477 (1982).
- ⁵⁶G. T. Surratt and A. B. Kunz, *Solid State Commun.* **23**, 555 (1977).
- ⁵⁷B. H. Brandow, *Adv. Phys.* **26**, 651 (1977).
- ⁵⁸E. Šimánek and M. Tachiki, *Phys. Lett.* **21**, 625 (1966).
- ⁵⁹The transfer integrals listed in Ref. 1 are those for the energy bands of NiO where the O 2*p* and Ni 3*d* levels are located at $\epsilon_p \sim -1$ eV and $\epsilon_d \sim 5$ eV (Table III). In order to calculate the valence-band spectrum of NiO, we must use LCAO parameters for energy bands with $\epsilon_p \sim -4$ eV and $\epsilon_d \sim \epsilon_p + \delta E_B \sim -8$ eV, where energies are measured relative to E_F . It has been assumed that when the energies of two orbitals are shifted in the opposite directions by the same amount, the transfer integral between them is not changed.
- ⁶⁰P. A. Cox, *Structure and Bonding* (Springer, Berlin, 1975), Vol. 24, p. 59.
- ⁶¹P. S. Bagus, J. L. Freeouf, and D. E. Eastman, *Phys. Rev. B* **15**, 3661 (1977).
- ⁶²G. Grenet, Y. Jugnet, T. M. Duc, and M. Kilber, *J. Chem. Phys.* **74**, 2163 (1981).
- ⁶³S. P. Kowalczyk, L. Ley, R. A. Pollack, and D. A. Shirley, as cited in Ref. 57.
- ⁶⁴G. Kuwabara, *Phys. Rev.* **138**, A99 (1965); T. Nasu, Ph.D. thesis, University of Tokyo, 1963 (unpublished).
- ⁶⁵K. W. Blazy, *Physica (Utrecht)* **89B**, 47 (1977).
- ⁶⁶D. Reinen, *Ber. Bunsenges, Phys. Chem.* **69**, 82 (1965).
- ⁶⁷J. H. Scofield, *J. Electron Spectrosc. Relat. Phenom.* **8**, 129 (1976).
- ⁶⁸L. C. Davis and L. A. Feldkamp, *Phys. Rev. B* **23**, 6239 (1981).
- ⁶⁹Other matrix elements were approximated as
- $$\sqrt{2}\langle \underline{c}d^9 | \tilde{H} | \underline{c}d^{10}\underline{L} \rangle = \sqrt{2/3}\langle d^7 | \tilde{H} | d^8\underline{L} \rangle$$
- $$= (2/\sqrt{3})\langle d^8\underline{L} | \tilde{H} | d^9\underline{L}^2 \rangle = \langle d^8 | \tilde{H} | d^9\underline{L} \rangle,$$
- considering effects of the different 3*d*-electron and ligand-hole numbers. Further, we assumed
- $$\langle d^9\underline{L} | T | d^8\underline{L}\epsilon f \rangle = [3/(2\sqrt{2})]\langle d^8 | T | d^7\epsilon f \rangle,$$
- $$\langle d^9\underline{L} | T | \underline{c}d^{10}\underline{L} \rangle = (1/\sqrt{2})\langle d^8 | T | \underline{c}d^9 \rangle,$$
- and
- $$\langle d^8\underline{L} | (e^2/r) | \underline{c}d^{10}\underline{L} \rangle = (\sqrt{5}/2)\langle d^7\epsilon f | (e^2/r)\underline{c}d^9 \rangle.$$
- ⁷⁰Y. Sakisaka, T. Ishii, and T. Sagawa, *J. Phys. Soc. Jpn.* **36**, 1365 (1974).
- ⁷¹T. Ishii, Y. Sakisaka, T. Matsubara, S. Sato, and T. Sagawa, *Solid State Commun.* **13**, 281 (1973).
- ⁷²G. Kuwabara and K. Aoyagi, *Jpn. J. Appl. Phys. Suppl.* **4**, 627 (1965).
- ⁷³J. Hugel and C. Carabatos, *J. Phys. C* **16**, 6713 (1983); **16**, 6723 (1983).
- ⁷⁴Y. M. Ksendzov and I. A. Drabkin, *Fiz. Tverd. Tela (Leningrad)* **7**, 1884 (1965) [*Sov. Phys.—Solid State* **7**, 1519 (1965)].
- ⁷⁵M. A. Wittenauer and L. L. van Zandt, *Philos. Mag. B* **46**, 659 (1982).
- ⁷⁶J. Kanamori, in *Electron Correlation and Magnetism in Narrow-Band Systems*, edited by T. Moriya (Springer, Berlin, 1981), p. 102.
- ⁷⁷G. A. Sawatzky and A. Lenselink, *J. Chem. Phys.* **72**, 3748 (1980).
- ⁷⁸O. Gunnarsson and K. Schönhammer, *Phys. Rev. B* **28**, 4315 (1983).
- ⁷⁹J. W. Allen, S.-J. Oh, M. B. Maple, and M. S. Torikachvili, *Phys. Rev. B* **28**, 5347 (1983).